Energies **2015**, *8*, 11846-11870; doi:10.3390/en81011846

OPEN ACCESS

energies

ISSN 1996-1073

www.mdpi.com/journal/energies

Article

A New Building-Integrated Wind Turbine System Utilizing the Building

Jeongsu Park [1,†], Hyung-Jo Jung [1,†,*], Seung-Woo Lee [2,†] and Jiyoung Park [3,†]

[1] Department of Civil and Environmental Engineering, Korea Advanced Institute of Science and Technology (KAIST), Daejeon 305-701, Korea; E-Mail: gemplx66@kaist.ac.kr

[2] TESolution Co. Ltd., Sungdu-Ri 724-12, Gongdo-Eup, Anseong-Si, Gyunggi-Do 456-825, Korea; E-Mail: swlee@tesolution.com

[3] Division of Architecture, Inha University, Incheon 402-751, Korea; E-Mail: jypark@inha.ac.kr

† These authors contributed equally to this work.

* Author to whom correspondence should be addressed; E-Mail: hjung@kaist.ac.kr; Tel.: +82-42-350-3626; Fax: +82-42-350-3610.

Academic Editor: Frede Blaabjerg

Received: 10 August 2015 / Accepted: 15 October 2015 / Published: 21 October 2015

Abstract: This paper proposes an innovative building-integrated wind turbine (BIWT) system by directly utilizing the building skin, which is an unused and unavailable area in all conventional BIWT systems. The proposed system has been developed by combining a guide vane that is able to effectively collect the incoming wind and increase its speed and a rotor with an appropriate shape for specific conditions. To this end, several important design issues for the guide vane as well as the rotor were thoroughly investigated and accordingly addressed in this paper. A series of computational fluid dynamics (CFD) analyses was performed to determine the optimal configuration of the proposed system. Finally, it is demonstrated from performance evaluation tests that the prototype with the specially designed guide vane and rotor for the proposed BIWT system accelerates the wind speed to a sufficient level and consequently increases the power coefficient significantly. Thus, it was confirmed that the proposed system is a promising environment-friendly energy production system for urban areas.

Keywords: building integrated wind turbine (BIWT); wind energy; guide vane; computation fluid dynamics (CFD); wind tunnel test

1. Introduction

Wind, one of the renewable energy sources, is so sustainable and environmentally friendly that the relevant market has increased every year with an annual growth of around 20% [1]. The common application for the use of wind energy is to construct wind farms, *i.e.*, arrays of large wind turbines, in hilly or coastal areas that have a constant flow of non-turbulent wind. In spite of its effectiveness, however, a wind farm has a critical limitation due to the long distance between the farm, which is usually located in a remote place, and an urban area, where over 60% of global energy demand is consumed. This long distance between the producer and the consumer requires an electricity transmission system that results in considerable energy loss during the transmission process and costs much money (e.g., $177,000/MW for capital cost of station equipment and $429/MW-km for transmission system [2]). These issues, electricity loss and high cost of the transmission system, should be accordingly addressed so that a more effective utilization of wind energy can be achieved in urban areas.

Because of the limitations of using rural wind farms, interest in directly utilizing wind energy within urban areas has gradually increased. However, wind environments in urban areas are quite different from those in hilly or coastal areas. First, wind speed in urban areas is generally less than that at the same height in hilly or coastal areas due to the surface roughness caused by complicated building arrangements. Furthermore, space needed to install many large wind turbines is limited in urban areas, so a wind farm may not be seen as a feasible approach in such areas. On the other hand, the upper air in urban areas is not considerably affected by surface roughness. In addition, specific building arrangements such as urban canyons or height differences between neighboring building structures can frequently create strong winds around buildings [3,4]. For example, in Hong Kong, the mean wind speed at 150 m is around 5 m/s to 6 m/s for a 50% probability of exceedance [5]. Thus, these attractive characteristics should be carefully examined when the use of wind energy in urban areas is considered.

Based on the above research background, high-rise buildings can be considered as one possible candidate for utilizing wind energy in urban areas. Some researchers have already investigated the feasibility of a building that incorporates wind turbines (or building-integrated wind turbines (BIWTs)) by conducting numerical simulations and estimating that the BIWT system would produce almost 20% of the necessary energy for the building operation [6]. Nowadays, interest in BIWT systems is considerably increasing and several buildings have introduced or are considering introducing BIWT systems inside their structures.

The application of BIWT systems to high-rise buildings can be done in two different ways. The first is to apply one or a few large-size wind turbines to high-rise buildings. As illustrated in Figure 1a, there are three possible locations for large-size wind turbines: (i) on the rooftop; (ii) between two adjacent buildings; and (iii) inside a hole within a building that is specially designed for this purpose. These types have already been applied to full-scale buildings such as the World Trade Center in Bahrain and Pearl River Tower in Guangzhou. Despite their high efficiency, however, it has been reported that they had several unsolved issues, such as noise and vibration problems caused by the large turbines and aesthetic dissatisfaction [7]. Above all, these types need structural strengthening to resist the additional force from the wind turbines being subjected to wind loads on the rooftops or between the adjacent buildings; therefore, they cannot be directly applied to existing buildings without

structural modification. In addition, to concentrate wind flows efficiently on a particular zone where turbines are installed, special care must be taken in the planning and design stages.

The second way to apply BIWT systems to buildings is to install many small-size wind turbines on the buildings instead of a few large-size wind turbines. Figure 1b represents the schematics of this approach and a full-scale application example of a real structure. This type of the BIWT system is considered as a convenient and economical method. One advantage of this approach is that it can be used with existing structures without any specific structural strengthening. However, the total output power from this system would be considerably lower than that from large-size wind turbines because their installable area is limited to such areas as rooftops and edges of buildings.

This paper proposes an innovative BIWT system that directly utilizes the building skin (or an exterior wall of a building) that is always subjected to wind pressure but is an unused large area, which is the case of all the conventional BIWT systems. To this end, we developed the proposed system by combining a guide vane that can concentrate the wind flow and increase its speed and a rotor with an appropriate shape for the designed guide vane. In this study, we thoroughly investigated and addressed several important design issues for the guide vane as well as for the rotor. A series of computational fluid dynamics (CFD) analyses was also carried out to determine the optimal configuration of the proposed system. Finally, the feasibility of the proposed system was experimentally validated by conducting wind tunnel tests with a prototype of the proposed system.

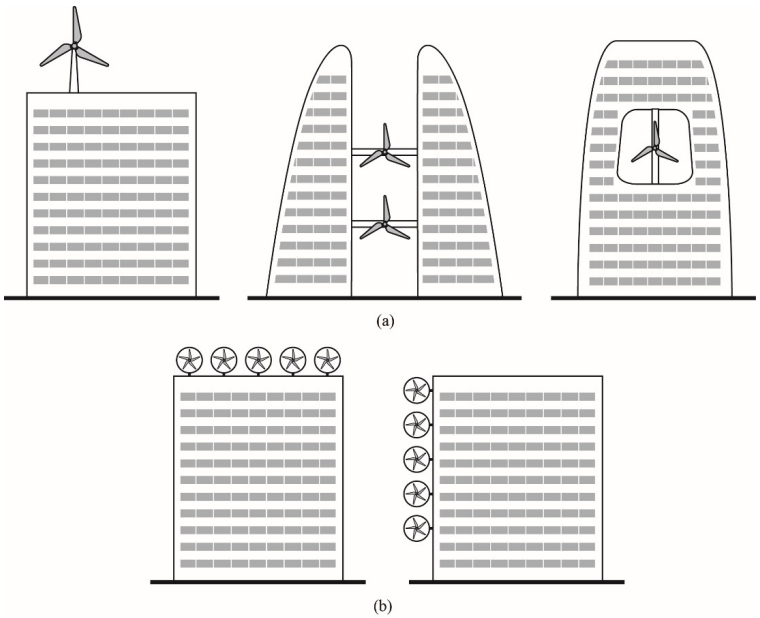

Figure 1. Building-integrated wind turbine system using wind turbines: (**a**) three possible installation locations of large-size wind turbines; and (**b**) two possible installation locations of small-size wind turbines.

2. The Proposed Building-Integrated Wind Turbine (BIWT) System

2.1. The Proposed System

A schematic diagram of the proposed system is shown in Figure 2. As shown in the left figure, the whole system is an assemblage of many unit modules filling an empty building skin area except

for windows. Modularization enables the system to be easily applied to various types of existing buildings and makes it convenient for the system to be attached and detached. The right picture in Figure 2 depicts a unit module consisting of a guide vane and a rotor. In the unit module, the guide vane is the key composition that changes according to approaching wind conditions, such as low velocity or high static pressure, to be appropriate for rotor operation. The characteristics of the wind flow around the building skin are very complicated. Every building has its own particular wind flow around itself due to its form and arrangement with neighboring structures. To concentrate the dispersed wind flow into a rotor efficiently, a guide vane should be introduced in the proposed system and plays an important role in increasing the wind speed. It is known that the generated power is proportional to the cube of the inlet speed, so an increase in the inlet wind speed is strongly related to the improvement of the system. Additionally, a series of guide vanes form empty space between themselves and the building skin. The empty space behind the guide vanes plays the role as a passage for the wind passing through the rotor to flow out of the building easily. It creates a pressure difference between the back and forth of the guide vanes and the wind effectively comes into the guide vane [8]. It is an important role for the proposed system because it is installed on the building skin where the wind velocity is relatively low and the static pressure is higher than on the edge of the building.

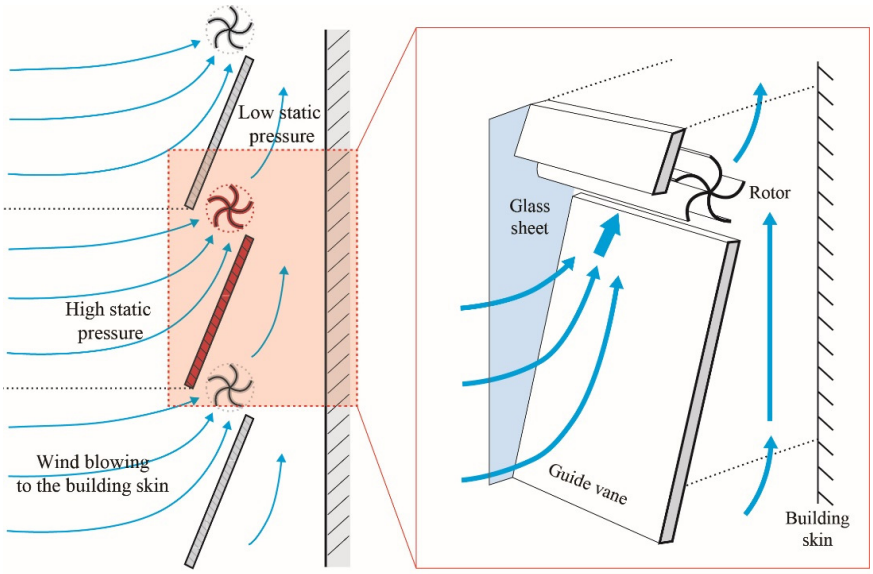

Figure 2. Schematic diagram of the proposed system.

The rotor is a main part of wind turbines, so selecting the optimal rotor is also important. Rotors are classified as the horizontal-axis type and the vertical-axis type according to the axis orientation. They also can be divided into the drag-force type and the lifting-force type based on how the rotor blades obtain the driving force [9]. It is generally known that wind turbines that use the lifting force have a higher efficiency. For the proposed system, however, the rotor is ought to be located between the guide vane and the building skin, so its diameter is limited. If diameter of the rotor is smaller, the tip speed of the rotor becomes lower with same operation revolution per minute (RPM) and it leads lower lift force on the blades because the lift coefficient of the blade decreases with wind speed; blades using the lifting force are inappropriate because they require a long diameter to achieve high performance. On the other hand, a Savonius rotor is operable even with a small diameter.

Note that most small-size wind turbines with a diameter smaller than 1 m use Savonius-type rotors. For this reason, a Savonius rotor, which operates on a vertical axis using the drag force, was selected in this study. In the following sections, several design strategies using CFD analyses were considered to obtain the final form of the guide vane and the blade, and the final design of the proposed system is validated through wind tunnel tests.

2.2. Advantages over Conventional System

2.2.1. Installable Area

As mentioned previously, structural strengthening or modification is usually needed to apply the conventional wind turbines to buildings, especially large-size turbines. Further, their deployable space (or area) on a high-rise building is limited to its rooftop and edges (sides). The basic concept of the proposed system can be graphically addressed as shown in Figure 3 by comparing the deployable space of the proposed system with that of the conventional wind turbine system. As shown in the figure, the conventional BIWT systems generally consist of one or a few large-size turbines or aligned small-size turbines following the edge, so they can be considered as 0- or 1-dimensional deployment. As a countermeasure, the proposed BIWT system consisting of many unit modules is designed to be installable on the building skin (or an exterior wall of a building), which is a previously unused and unavailable large area (see Figure 3). The ideal window to wall ratio for energy consumption is reported as 25% to 30% [10,11] so there remains large installable area except for windows. Different from the conventional BIWT systems, the proposed system can be considered a two-dimensional deployment.

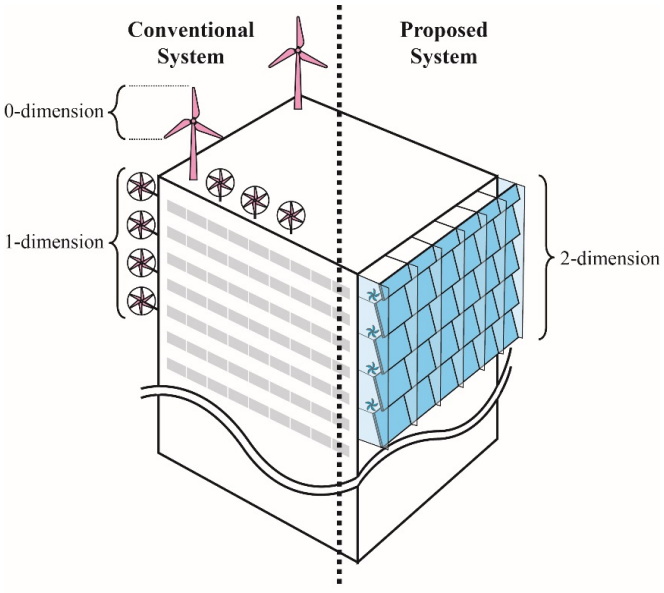

Figure 3. Comparison of the installation area between the proposed system and the conventional ones.

2.2.2. Structural Issue

Conventional BIWT systems occasionally require structural reinforcement because the additional wind pressure acts on the wind turbine installed on the rooftop or between buildings. However,

the proposed system is able to utilize the wind pressure acting on the building wall, so structural strengthening or modification is not necessary because this wind pressure is already considered in the building design stage as shown in Figure 4 (e.g., the wind velocity for the design wind load in Seoul, Korea is regulated as 30 m/s by Standard Design Loads for Buildings.). The only important consideration is a structurally solid connection between the modules and the building skin for the system to satisfy the standard as a cladding.

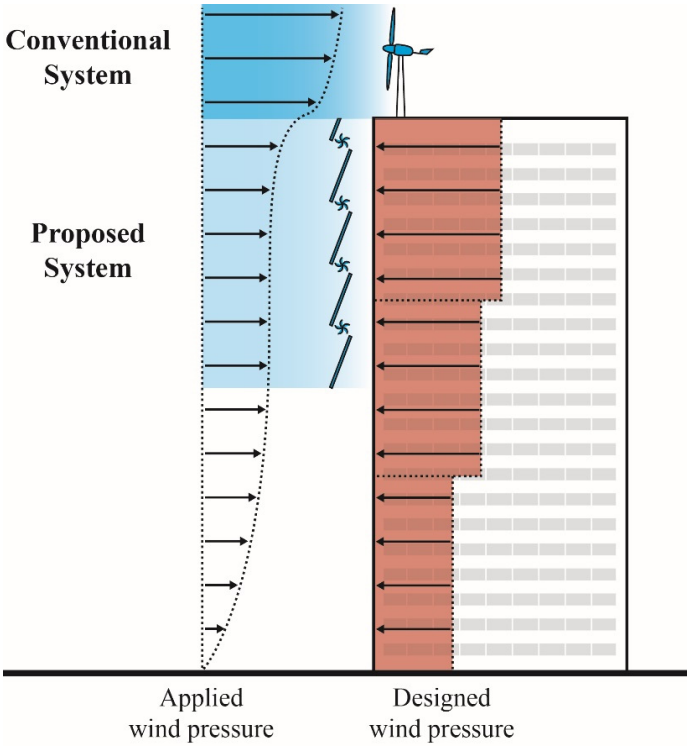

Figure 4. Structural aspect of the proposed system.

2.2.3. Urban Environment

The guide vane of the proposed system conceals the rotor inside the system so that it is not exposed to the outside. Different from the conventional systems, it is able to hide the blade from the pedestrian's view, so it is not aesthetically unpleasant. The noise generated during operation, one of the biggest issues for application in residential environments, can be reduced using a Savonius rotor, which has a lower noise level and lower cut-in speed compared to other types, especially horizontal axis types [12,13]. In addition, it reduces emissive noise around the building because the rotor is concealed by the guide vane.

3. Design of Proposed System

3.1. Guide Vane

3.1.1. Design Issue for Shape of Guide Vane

To determine the shape of the guide vane in the proposed system, we assumed that the system would be deployed in the building's upper part because the approaching wind speed is faster in

that region. Note that above the stagnation point on a building's windward wall, which is 70% of the building height, the wind flows toward the upper floors [14]. Inclination of the guide vane helps to efficiently collect the upward wind as it climbs over the building skin.

Several researchers have explored methods for increasing wind turbines' efficiency using special equipment: A guide vane, a wind concentrator, a duct or a convergent nozzle [15–17]. Their first strategy was to increase wind velocity passing via a nozzle before the wind reached the rotor. Wind speed is a very important condition for the wind turbine to generate sufficient power because it is proportional to cubic of inlet velocity. The researchers have proved that a smaller area ratio, defined as the ratio of an outcome to an income area, leads to faster wind exiting the nozzle. Another strategy is blocking half of the rotor from the upcoming wind. This blocking apparatus gets rid of the negative torque from the opposite direction of the operation rotation of the rotor, resulting in the improvement of a wind turbine's efficiency.

Two improvement strategies were used in designing the guide vane of the proposed system. The bottom face of the upper guide vane and the top face of the lower module form the shape of the nozzle as illustrated in the right picture in Figure 5. Additionally, the shape of the proposed system was determined by the position of the rotor, which depends upon the rotating direction. In the Figure 5, two models, Types 1 and 2, are illustrated and have the same front shape marked with a red bold line but a different rear shape due to the rotor arrangement. In comparing the two models, Type 2 has better features than Type 1 from the point of view of space. As mentioned in the previous section, forming enough space behind the guide vane is directly related to the system's efficiency. If the distances between the guide vane and the building skin of Types 1 and 2 are the same, Type 2 forms a larger space behind the guide vane as shown in Figure 5. In addition, it is expected to be lightweight thanks to its small cross sectional area. For these reasons, Type 2 was chosen as the final shape.

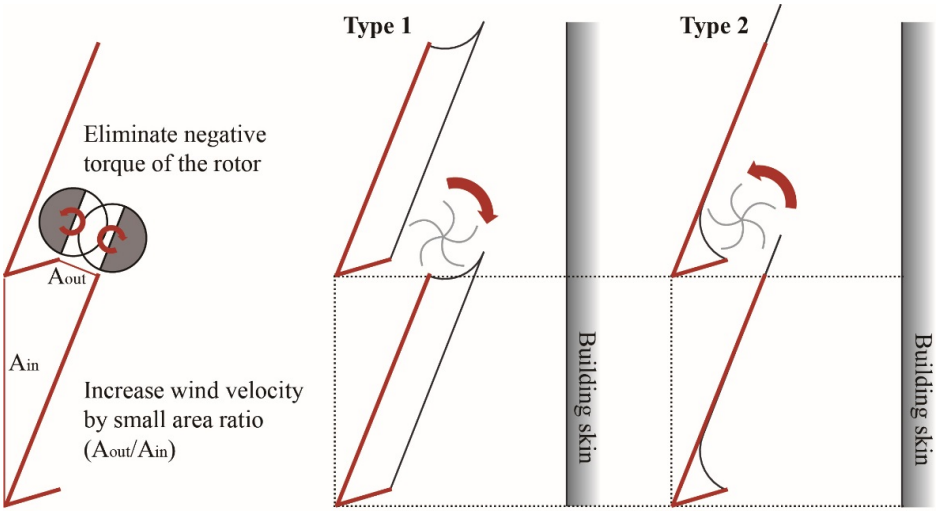

Figure 5. Design issues for the shape of the guide vane.

3.1.2. Design Issue for Dimension of Guide Vane

The larger the module size and distance between the guide vane and the building skin, the higher the generated power. For this study, the most efficient shape for the proposed system was examined considering the limited volume. For this reason, a module is assumed to be installed in a cube whose

side is 1 m. The distance between the upper and lower modules, the distance between the building skin and the module, and the width of the module were designed to be 1 m. The other dimensions of the guide vane were determined by the rotor diameter. Generally, the performance of a wind turbine increases with the rotor diameter because the torque applied to the rotor is proportional to the swept area. It is also not operable, irrespective of the wind speed, if the rotor diameter is too small. In the proposed system, however, an increase of the rotor diameter causes a decrease of the inlet wind velocity due to the large area ratio of the nozzle shape and lack of the space behind the rotor. To determine its diameter, CFD analyses were conducted with several guide vane models. Four installable rotor diameters, 20 cm to 50 cm, were selected and the other dimensions of the targeted guide vane models were determined based on the diameter as illustrated in Figure 6.

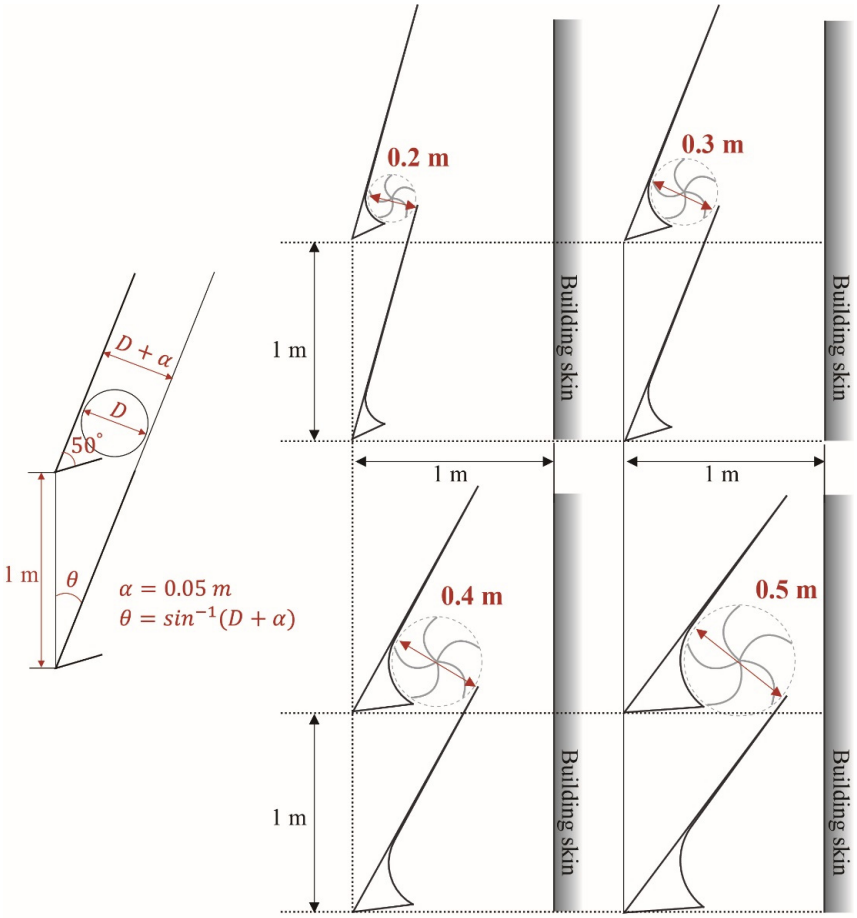

Figure 6. Design issues for the dimensions of the guide vane.

3.1.3. Computational Fluid Dynamics (CFD) Analysis

To compare the performance of the four guide vane models designed in Section 3.1.2, CFD analyses were performed. The purpose of the analyses was to compare their performance according to wind speed, not to find out the exact value so a two-dimensional domain was used to save calculation time in the domain illustrated in Figure 7. Five guide vanes were assumed to be installed in a line on the upper building skin. The boundary condition "velocity inlet" was applied at the entrance, the "wall" at the modules and the building, and the "pressure outlet" at the outlet, and quadrilateral cells are were created in the modeled domain.

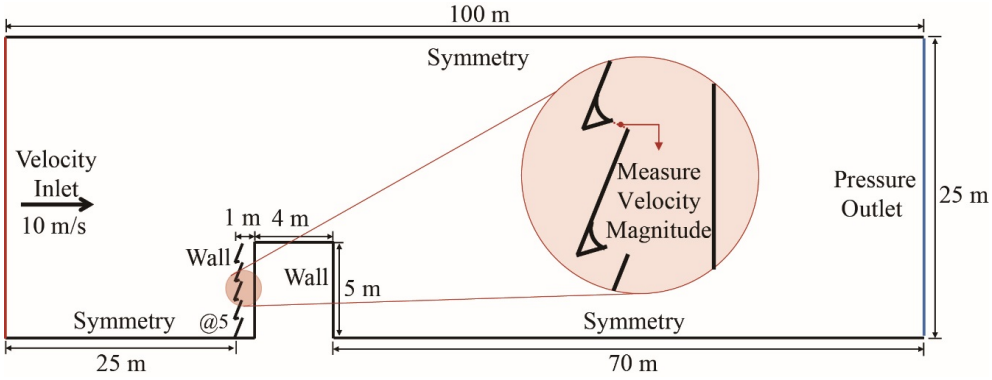

Figure 7. Computational fluid dynamics (CFD) simulation domain for the guide vane analyses.

The computations were performed using a Navier–Stokes solver. The CFD simulation conditions are described in Table 1. After the simulation was finished, the wind velocity magnitudes were measured on the outlet point of the third module. The torque on the center of the rotor generated by outlet wind was used as valuation criteria; it was calculated using the equation below [9]. ρ is the air density, A is the swept area, r is the rotor radius, and v is the wind velocity magnitude on the outlet point:

$$T = \frac{1}{2}\rho A v^2 \cdot r \quad (1)$$

The results from the guide vane models were compared as shown in Figure 8. When the diameter was 20 cm, the guide vane increased wind speed dramatically due to the small area ratio. However, the swept area of the rotor was too small to generate the corresponding torque value with wind velocity. When a diameter was 50 cm, the guide vane poorly performed because of the narrow space behind the guide vane. Consequentially, the torque was not as significant as with other models. Among the targeted models, the guide vane designed for the rotor with a diameter of 30 cm showed the most efficient performance, so it was selected for the final model.

Table 1. CFD simulation conditions for the guide vane analyses.

Computational Conditions	Value	Computational Conditions	Value
Space/time	2D/Steady	Interpolating scheme (turbulence)	Second order upwind
Viscous model	k-omega (Standard)	Inlet *X*-velocity	10 m/s
Density	1.225 kg/m^3	Inlet *Y*-velocity	0 m/s
Viscosity	1.7894×10^{-5} Pa·s	Inlet/outlet turbulent intensity	10%
CFD Algorithm	SIMPLE	Inlet/outlet hydraulic diameter	1 m
Interpolating scheme (momentum)	QUICK	Residuals	5.0×10^{-4}

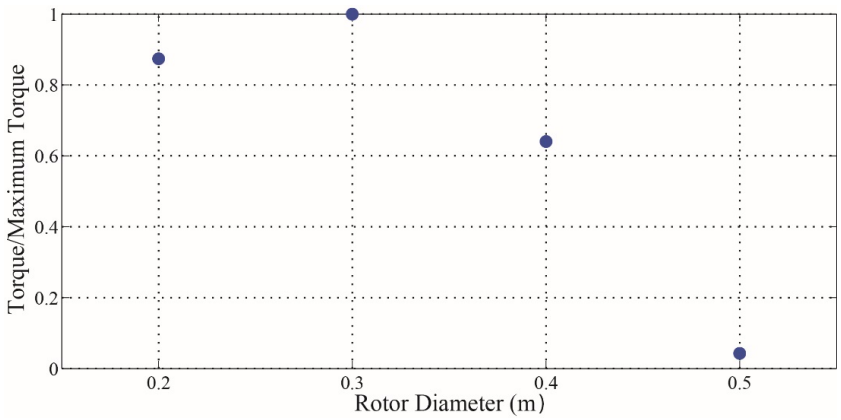

Figure 8. Torque generated on the center of the rotor zone.

3.2. Rotor

3.2.1. Design Issue for Rotor

A vertical-axis wind turbine is categorized as Savonius, Darrieus, or Giromill according to whether their blades obtain a drag force or a lift force. A Savonius rotor operates using a drag force that is converted into the torque on a rotating shaft. Although it is known for a lower power coefficient than other vertical-axis wind turbines using the lift force, this type of a turbine has several advantages, such as low noise and angular velocity in operation and reduced wear on moving parts, which are suitable features for residential environments.

The power coefficient of a Savonius rotor is directly related to the shape and number of blades. It is known that a Savonius rotor with a gap between two or three semicircular blades has the highest efficiency in an open place such as a field or roof [12]. For the proposed system, however, the rotor is installed in front of the building skin so the conditions around the rotor in the proposed system must be carefully taken into consideration to create a proper rotor design. First of all, the available diameter of the rotor is restricted because it is installed between the guide vane and building skin. This is one of the main reasons why the Savonius-type rotor was selected in the proposed system. Second, the over half the rotor area is hidden from driving wind force to prevent a negative torque so it is difficult to get a stable performance with only two blades. Finally, the rotor is enveloped by walls such as the building skin and guide vane. The vacant space between blades can be a solution for wind to pass out of the rotor efficiently, thus extending the wind passage.

We chose several types of Savonius rotors with different shapes and numbers of blades from previous studies and performed CFD analyses to compare their performances. The schematics of the rotor models are shown in Figure 9. All rotors were assumed to have a diameter of 30 cm and a thickness of 2 mm considering the manufacturable size of a rotor. Rotor A has three blades with over gap, which is known as one of the models showing the highest performance for open space [18]. Rotor B has three particular-shaped blades and it is a merchandised model called GWE-200BI by Goldwind Energy in South Korea. Rotors C to F are not merchandised models but the shapes of the blades are referenced from previous studies [19,20].

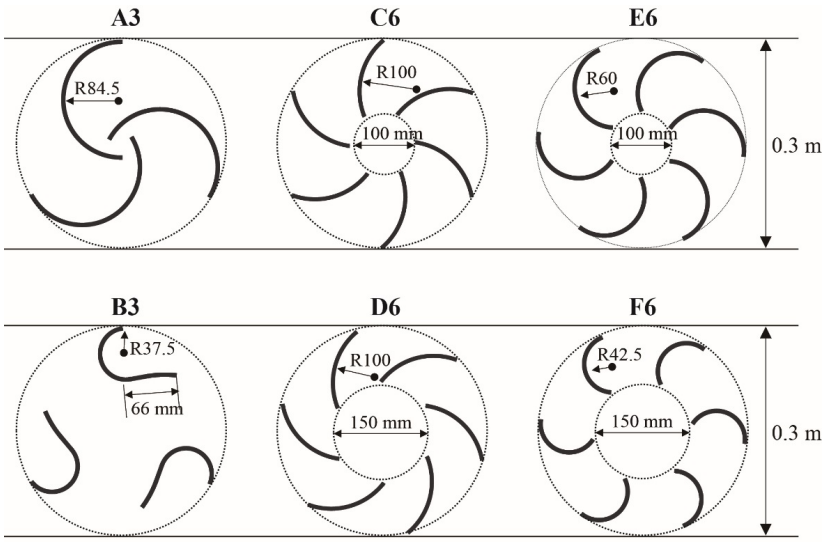

Figure 9. Cross sectional diagrams of the rotors considered in this study.

3.2.2. Computational Fluid Dynamics (CFD) Analysis

The rotor installed on the module had a high aspect ratio, so unsteady two-dimensional analyses were conducted to shorten the computing time. For the same reason, the domain is also reduced as illustrated in Figure 10. Our analysis method followed the previous research performed by Dobrev *et al.* [21]. Target rotors were located between the guide vanes representing the assembled three modules and sliding mesh was applied around the rotors to represent the rotation. The boundary condition "velocity inlet" was imposed at the entrance, "wall" was applied behind the modules to represent the building skin, and "pressure outlet" at the corner of the building skin. The gap between the lowest guide vane and the building skin was the "velocity inlet" to represent wind coming up from lower modules. To ensure the *y*+ parametric values of the walls of the blades, every side was divided into 0.002 m. Additionally, 10 rectangular layers with a growth factor of 1.05 and a first height of 3×10^{-4} m were created around the blades. Quadrilateral cells were created on the whole area including moving mesh.

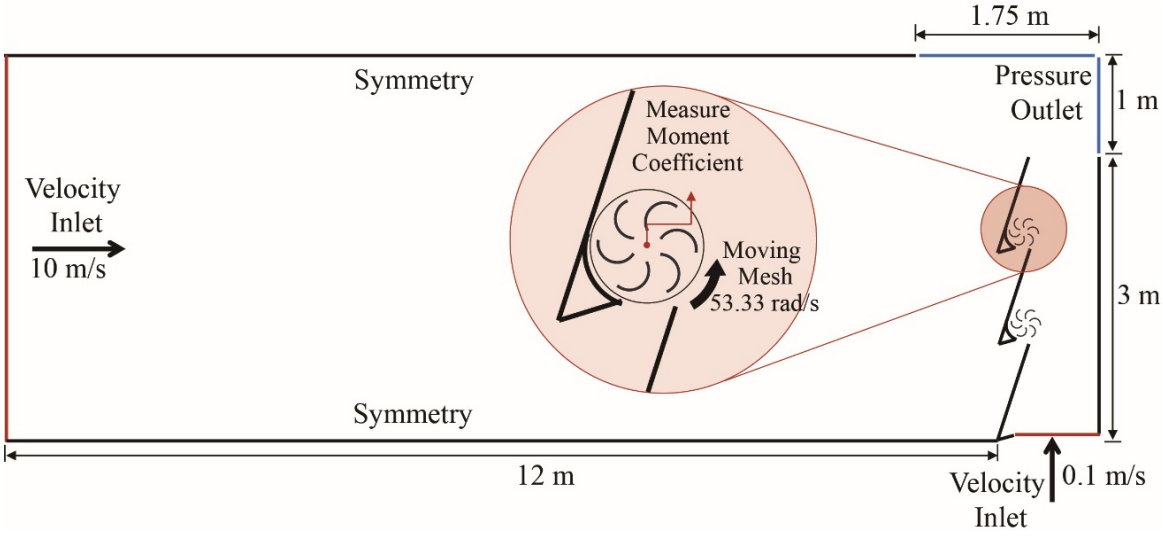

Figure 10. CFD simulation domain for the rotor analyses.

The computations were performed using the Navier–Stokes solver. The CFD simulation conditions were same as in Table 1, and additional conditions for unsteady simulation are described in Table 2. For the results, the torque applied on the center of each rotor was measured under same rotation condition. The moving mesh was rotating at 53.33 rad/s clockwise for the tip speed ratio (TSR) of the rotor to become 0.8, which is in the general TSR range for a Savonius rotor. Each time step was 2.39×10^{-4} s for the rotor to turn 1°. It was conducted until the rotor rotated four turns. Because the rotor performed unstably at first, the results during the last revolution were examined. The torque applied to the center of each rotor was measured and the average values during the last revolution were calculated. The torque performance of rotor F for the last revolution is shown in Figure 11.

Table 2. CFD simulation conditions for the rotor analyses.

Computational Conditions	Value	Computational Conditions	Value
Space/time	2D/Unsteady	Time stepping method	Fixed
Viscous model	k-omega (Standard)	Time step size	3.27×10^{-4} s
Blade motion type	Moving Mesh	Number of time steps	1440
Blade rotational velocity	53.33 rad/s	Residuals	3.0×10^{-4}

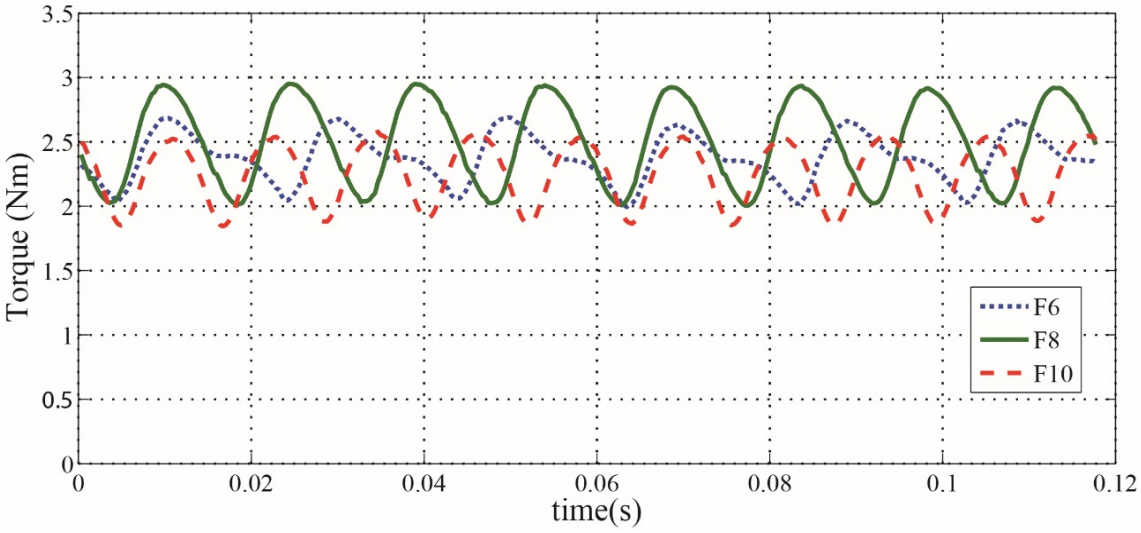

Figure 11. Torque generated on the center of rotor F for one rotation.

Figure 12 shows the average torque values of the target rotors divided by the most efficient model. As shown in the graph, there is not a definite trend toward the number of the blades or even for the same blade shape. We guess that this is because the features of the rotor, e.g., the gap between the blades and the tangential angle of the blades influence the performance of the guide vane and not only the rotor. Overall, the rotors with internal space have a higher performance and the rotors with many blades show more stable results with a smaller standard deviation value than others because a close formation of the blades makes the rotor easily generate drag force at any angular position. For these reasons, each blade model showed their peak efficiency with different number of the blades. Among the all target models, rotor F with eight blades had the highest performance so it was selected for the final design.

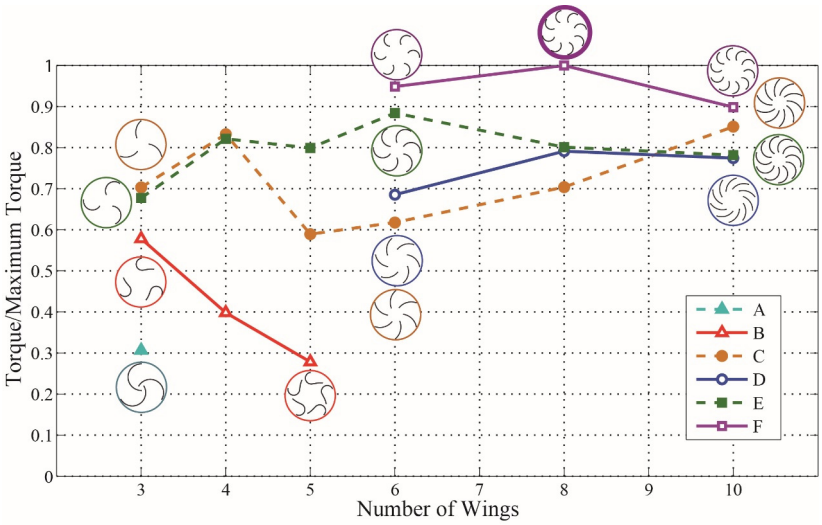

Figure 12. Average torque values generated on the center of the rotors.

4. Experimental Evaluation

The performance of the proposed system was evaluated through two-step experiments. The first step was a performance evaluation of the guide vane and the second step was of the rotor. First, a guide vane performance evaluation was conducted in a boundary layer wind tunnel. The purpose of the test was to examine wind velocity magnitude distribution inside the proposed system under constant approaching wind speed. After guide vane performance tests, the rotor performance was examined in a different wind tunnel with an operation wind speed higher than the previous one. These tests were aimed at examining the power coefficient of the rotor.

4.1. Experimental Evaluation of Guide Vane Performance

The efficiency of the proposed system is related to the performance of the guide vane. To validate the proposed shape of the guide vane, a series of wind tunnel tests with scaled modules were performed. A building model with a height of 1.5 m was manufactured considering the size of the boundary layer wind tunnel. To avoid impact of anemometers on wind flow, the scaled guide vane model must not be too small compared with the diameter of the sensors. For these reasons, nine modules with a height of 30 cm were mounted on the walls of a building model with three columns (Figure 13) and the wind velocity magnitude distribution around the center module was examined. The center scaled module represents the proposed system installed close to the stagnation point of the building skin where there are unfavorable conditions for wind turbines, such as high static pressure and low wind velocity. We chose the distance between the module and the building skin as 30 cm to have the same value as the unit module length. It was placed in the test zone of the boundary wind tunnel model, and its specifications are shown in Table 3. Hot wire anemometers were placed at 11 points around the center module for evaluating the performance of the module. The measurement points are described in Figure 14. Points 1 to 5 examine the wind speed increase inside the guide vane, Points 6 to 9 represent the rotor position, and Points 10 and 11 examine the wind ventilation behind the guide vanes. To measure the approaching wind speed, the reference point was located at 40 cm from the middle of the center module.

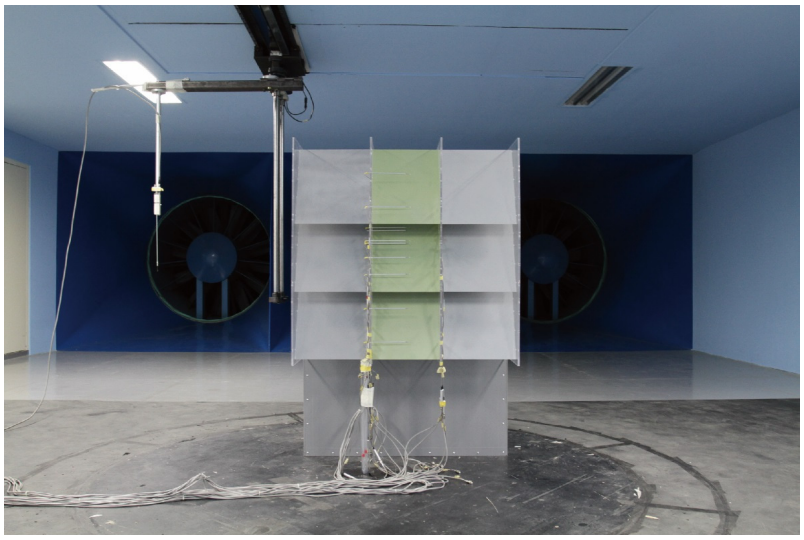

Figure 13. Scaled guide vane model.

Table 3. Specifications of the boundary layer wind tunnel.

Parameter	Value	Parameter	Value
Wind tunnel type	Eiffel type	Wind speed	0.3–11.5 m/s
Full length	36.825 m	Turbulence intensity	<0.5%
Test section size	8 (*W*) × 2.5 (*H*) × 23.2 (*L*) m	Wind velocity deviation	<1.0%

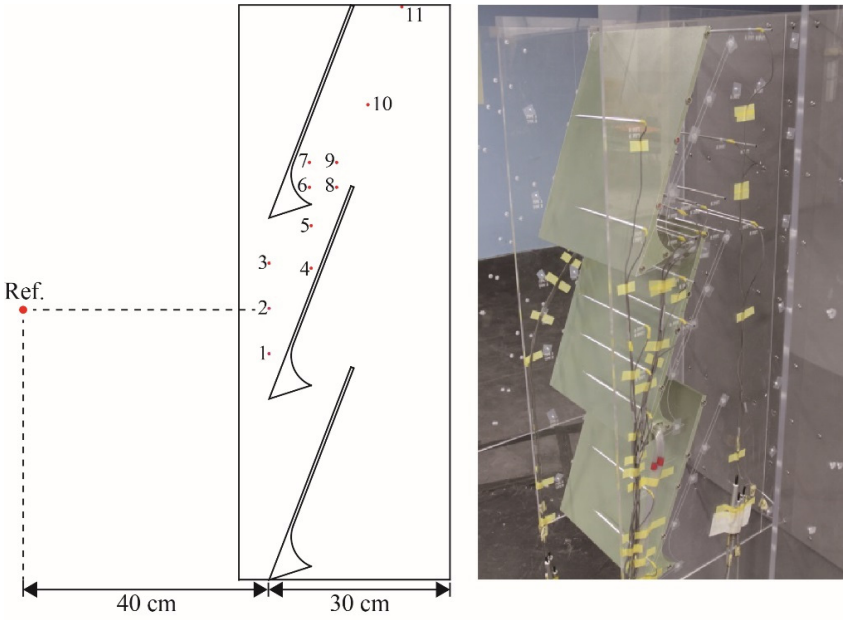

Figure 14. Measurement points on the scaled guide vane model.

The wind velocity magnitude was measured for different approaching wind speeds. The tests were performed under smooth flow conditions, so the turbulence intensity was maintained below 0.5%. The wind velocity ratio values, the point velocity divided by the reference wind velocity, are shown in Figure 15. The first graph is the group of points from the entrance to the exit of the guide vane. While the wind speed at the entrance drastically decreases, it increases up to almost two times the approaching velocity value. Compared with the entrance points, the guide vane augments wind speed

by over 300% under different incoming wind speeds. Our test results validate that the guide vane with the proposed shape concentrates wind flow effectively. The second graph gives the values of the points at the rotor position. At Points 6 and 7, the wind speed becomes almost zero because the guide vane blocks the incoming wind at these points. It shows that the guide vane effectively prevents negative torque generation on half of the rotor position. The last graph is the group of points behind the guide vane. The wind speed at the exit of the guide vane, Point 9, kept its velocity until it reached Point 11. Wind flows after the rotor rapidly passed through so low pressure behind the proposed system was maintained.

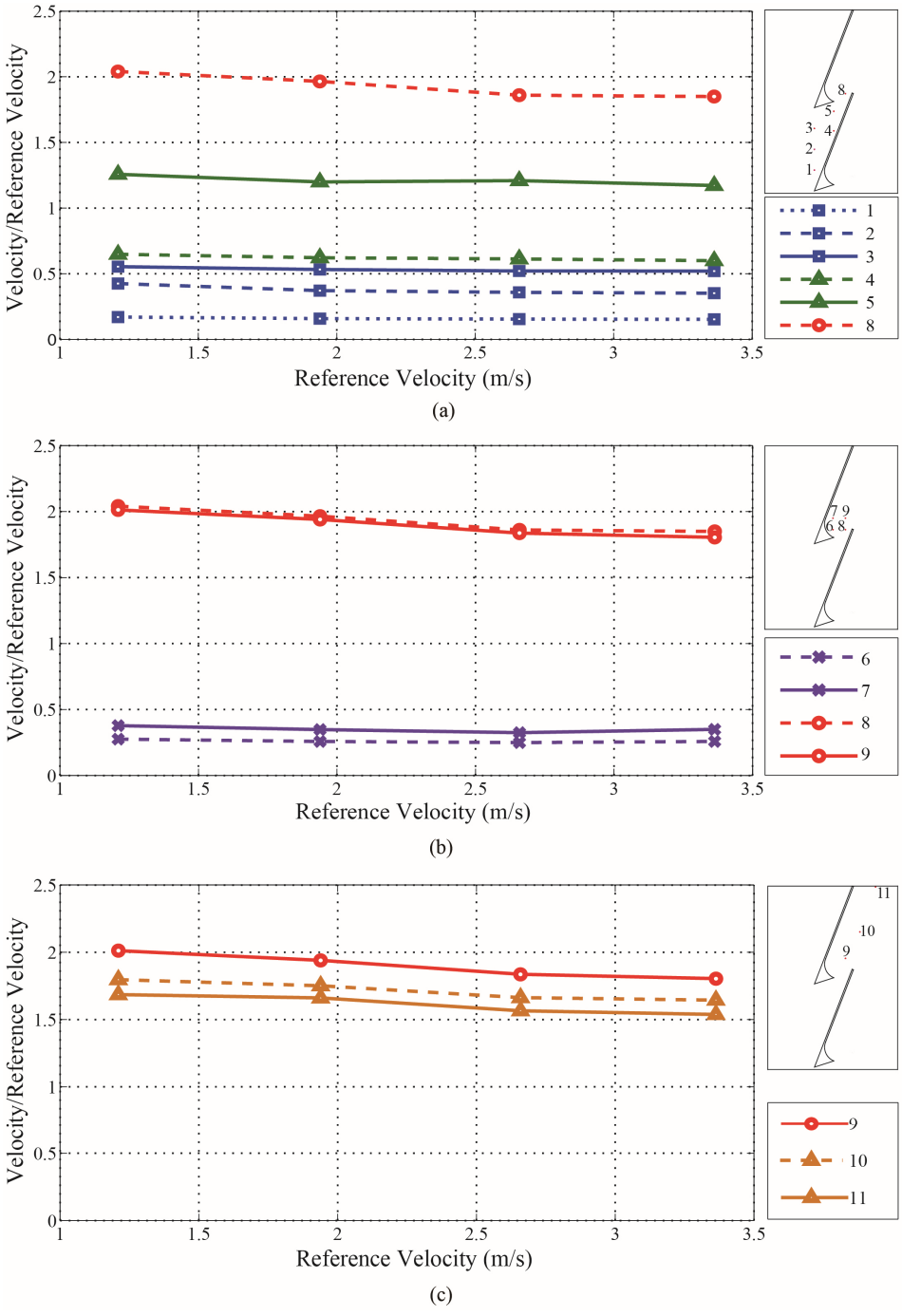

Figure 15. Wind velocity rate of the scaled guide vane model: (**a**) points before the rotor position; (**b**) points inside the rotor position; and (**c**) points after the rotor position.

4.2. Experimental Evaluation of Rotor Performance

A prototype was manufactured to examine the performance of the rotor. The width and height of one module were 1 m and the distance from the building skin to the module was also 1 m. Rotor F8, which had the most efficient performance in Section 3 was selected for the prototype. The parameters of the rotor are summarized in Table 4. A 200 W-capacity turbine was assembled with the rotor, and a three-phase AC to DC inverter and an electric load were set up to measure the generated power from the rotor. The manufactured guide vane and the rotor are shown in Figure 16a and an assembled diagram of the proposed system is illustrated in Figure 16b.

Table 4. Parameters of the rotor.

Parameter	Value	Parameter	Value
Diameter (m)	0.30	Number of blades	8
Length (m)	0.793	Weight (kg)	4.79
Material	AL.5052	-	-

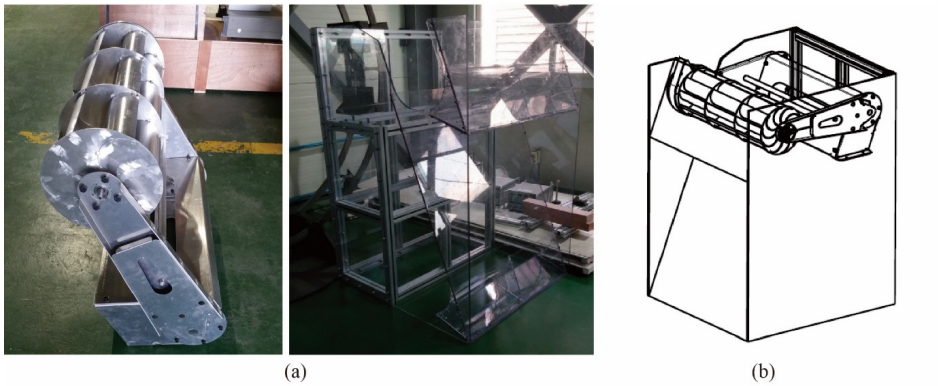

Figure 16. (**a**) Prototype model of the rotor and the guide vane and (**b**) assembly diagrams.

A small-scale wind tunnel was used for the performance tests and its specifications are shown in Table 5. During the tests, the turbulence intensity in wind tunnel was maintained below 0.5%. Before making the rotor performance evaluation, the guide vane of the prototype was only installed inside the wind tunnel and the wind speed at the outlet area (*i.e.*, outlet velocity), which represents Point 8 in the previous section, was measured. Finally, the rotor was installed in the prototype and its performance was evaluated. Figure 17a,b indicates the schematic diagram and the photo of the experimental setup, respectively. As shown in the figures, the prototype was laid inside the wind tunnel and a uniform wind was blowing from the entrance. The maximum power output was investigated with a changing electric load connected to the rotor.

When the rotor started its operation, the wind speed in front of the entrance of the guide vane was measured as 1.87 m/s, which is a relatively low value compared to the conventional Savonius rotors. The guide vane increased the wind speed in front of the rotor and enabled it to perform at a low cut-in speed. Further, it easily started to rotate at any angular location of the rotor because it had many blades. The rotor generated maximum power when its TSR was about 0.55 in different approaching wind speeds and the power output results are plotted against outlet velocity in Figure 18. The power generated from the rotor drastically increases as the approaching wind speed increases.

The power coefficients using the swept area of the rotor and the undisturbed wind speed were calculated at each wind speed and the average value was 0.381. The calculation power curve using the average power coefficient is also plotted in Figure 18 and it shows the power output is proportional to cubic of the outlet velocity.

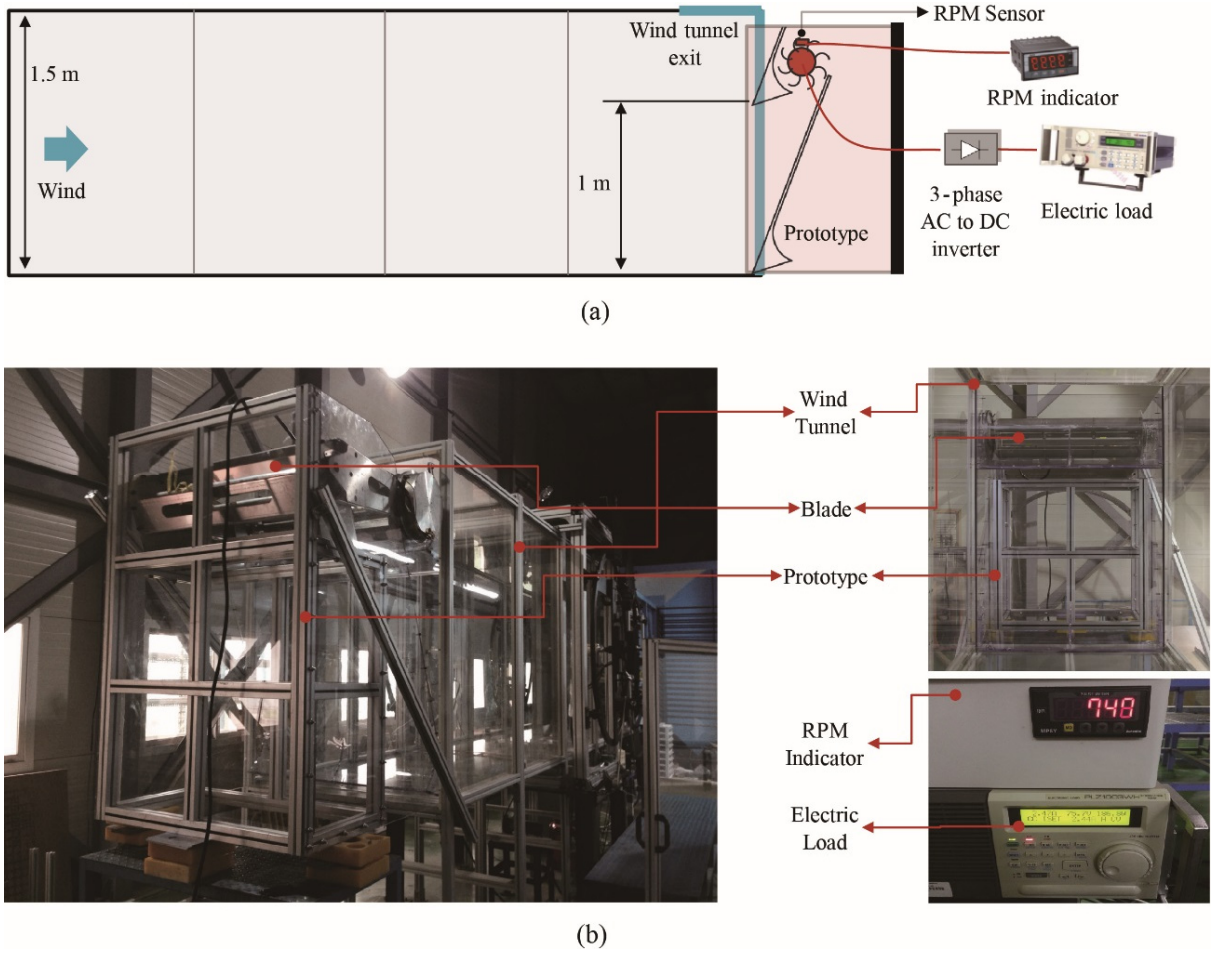

Figure 17. Experimental setup of the performance evaluation test: (**a**) schematic diagram; and (**b**) photo of the experimental setup.

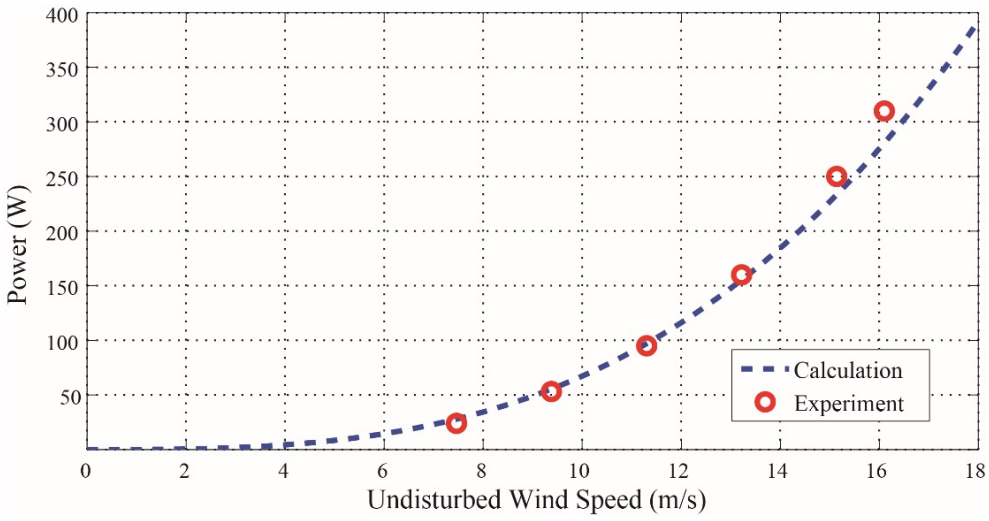

Figure 18. Generated power output.

Table 5. Specifications of a small scale wind tunnel.

Parameter	Value
Wind tunnel type	Two dimensional
Full length	17.297 m
Test section size	1.0 (*W*) × 1.5 (*H*) × 6.0 (*L*) m
Wind speed	0.3–21 m/s
Turbulence intensity	<0.5%

4.3. Discussion

The producible power generated by the proposed system is discussed using the annual electricity consumption of a residential building. Haeundae, Busan in South Korea was selected as a target area because many high-rise buildings exist there and much wind rises around them. In the targeted area, a 51-story building, with a height of 157 m, was reported to consume electricity of 36.42 kWh/m^2 for a year [22]. One floor of the building is 759.8 m^2, so the daily-consumed electricity by the whole building was estimated at 3860 kWh.

The estimated generated power from one module of the proposed system was calculated using daily average wind velocity and direction data in 2014 measured at a 10 m altitude in Busan by Korea Meteorological Administration (KMA) [23]. The estimation processes were as follows. First, the wind velocity at the stagnation point of the target building, *i.e.*, approximately 70% of the building height from the ground level, was predicted by Deacon wind profile in urban area [24]. Second, the power generated from one module of each day was calculated using the wind speed increase ratio of the guide vane from Section 4.1 and the power coefficient of the rotor from Section 4.2 when the wind of the average velocity continuously blew for a day. The daily average wind velocity data given by KMA and estimated power outputs are shown in the Tables A1–A12 in appendix. Third, the module was installed toward eight different azimuth and the daily powers corresponding with wind direction were summed during the season. We assumed the proposed system was affected by the wind blowing at the angle of ±45°. Seasonal average values per day are shown in Table 6.

Table 6. Seasonal expected power for Busan, Korea.

Season		Spring	Summer	Fall	Winter	Annual
Average wind velocity (m/s)		4.8	4.6	3.9	5.0	4.6
Estimated power per day (kWh)	N	0.060	0.086	0.148	0.270	0.140
	NE	0.058	0.096	0.152	0.166	0.118
	E	0.064	0.097	**0.154**	0.043	0.089
	SE	0.036	0.049	0.039	0.000	0.031
	S	0.323	0.350	0.040	0.031	0.187
	SW	**0.410**	**0.354**	0.063	0.161	**0.248**
	W	0.291	0.239	0.081	0.256	0.217
	NW	0.098	0.014	0.095	**0.342**	0.137

Among the eight azimuths, the proposed system installed toward southwest direction showed the most efficient performance. For this case, one module with an inlet area of one square meter produces 0.248 kWh/day for a year and 0.410 kWh/day especially in spring. Finally, the total

generated power from the whole system was calculated. The following assumptions were considered to estimate the installable area. First, the proposed system was installed above the stagnation point. Second, windows, where the modules are not installable on, dominate 25% of the building skin. Last, the floor plan of the building was a square so the length of the targeted side building was the square root of the one floor area. Thus, it was estimated that the proposed system would produce 241 kWh per day, which is about 6.3% of the daily-consumed electricity of the targeted building.

5. Conclusions

An innovative BIWT system that exploits wind pressure on a building skin was proposed. The proposed system consists of a guide vane that effectively collects the incoming wind and increases its speed, and a rotor with an appropriate shape for a specific condition. To obtain the most appropriate proposed system, several important design issues for the guide vane and the rotor were thoroughly investigated and accordingly addressed. In the investigating procedure, a series of CFD analyses were performed to determine the optimal configuration of the proposed system. Our CFD analyses verified that the guide vane designed for a rotor diameter of 30 cm had the best performance when the module was installed inside a cube with edges of 1 m in length. In addition, we verified that the eight-blade rotor with a spacious inner space (rotor F8) showed the best performance. Performance evaluation was made through two-step experiments. First, the guide vane performance was verified using the scaled guide vane modules. It was observed from the wind tunnel test that the wind was effectively augmented passing through the guide vane. For the next step, the performance evaluation test of the rotor was performed with the prototype of the proposed BIWT system and it was observed that the power coefficient of the rotor was 0.381. Finally, the estimated producible power from the system was compared with the energy consumption of a residential building; it was predicted that the proposed system can supply about 6.3% of needed electricity. In conclusion, our study verified that the proposed BIWT system is a promising environment-friendly energy production system for urban areas.

Acknowledgments

This work was supported by the New & Renewable Energy of the Korea Institute of Energy Technology Evaluation and Planning (KETEP) grant funded by the Korea government Ministry of Knowledge Economy (No. 20123030020090).

Author Contributions

Jeongsu Park is the principal researcher of this work. He conducted the numerical and experimental research. Seung-Woo Lee assisted wind tunnel tests and data analysis. Jiyoung Park participate in drafting the article or revising it. Hyung-Jo Jung supervised all of this research and give final approval of the version to be submitted and any revised version.

Conflicts of Interest

The authors declare no conflict of interest.

Appendix

Table A1. Estimated power output per day in January.

Date	1	2	3	4	5	6	7	8	9	10	11
Average wind speed (m/s)	5.3	2.7	2.4	2.7	2.9	2.5	3.1	2.8	4.1	2.9	2.6
Main wind direction	WSW	W	NNW	NNW	N	N	NNW	NNW	N	N	WNW
Estimated power output (kWh)	1.58	0.21	0.15	0.21	0.26	0.17	0.32	0.23	0.73	0.26	0.19
Date	12	13	14	15	16	17	18	19	20	21	22
Average wind speed (m/s)	2.5	3.5	4.2	3.6	4.1	3.0	3.3	3.4	4.7	4.4	4.3
Main wind direction	N	NNW	NNW	N	NNW	NNW	NNW	NNW	WNW	WNW	NNW
Estimated power output (kWh)	0.17	0.46	0.79	0.50	0.73	0.29	0.38	0.42	1.11	0.91	0.85
Date	23	24	25	26	27	28	29	30	31		
Average wind speed (m/s)	3.6	5.9	4.8	3.1	3.2	4.0	3.3	5.0	1.9	-	-
Main wind direction	NNW	W	SW	N	W	WSW	SW	W	NW	-	-
Estimated power output (kWh)	0.50	2.19	1.18	0.32	0.35	0.68	0.38	1.33	0.07	-	-

Table A2. Estimated power output per day in February.

Date	1	2	3	4	5	6	7	8	9	10	11
Average wind speed (m/s)	2.6	3.9	3.7	4.5	3.3	3.1	4.6	3.5	3.6	4.4	3.9
Main wind direction	WSW	SSW	N	N	NNW	NE	NE	NE	NNE	NNE	NNE
Estimated power output (kWh)	0.19	0.63	0.54	0.97	0.38	0.32	1.04	0.46	0.50	0.91	0.63
Date	12	13	14	15	16	17	18	19	20	21	22
Average wind speed (m/s)	3.7	4.0	4.9	3.6	2.2	3.7	4.3	3.8	2.5	3.3	1.8
Main wind direction	NNE	NNE	NNE	NNW	SSW	NE	NE	NNE	WSW	NNW	SSW
Estimated power output (kWh)	0.54	0.68	1.25	0.50	0.11	0.54	0.85	0.58	0.17	0.38	0.06
Date	23	24	25	26	27	28					
Average wind speed (m/s)	2.2	2.7	2.8	3.1	3.2	3.1	-	-	-	-	-
Main wind direction	SW	SSW	N	NE	NNE	NE	-	-	-	-	-
Estimated power output (kWh)	0.11	0.21	0.23	0.32	0.35	0.32	-	-	-	-	-

Table A3. Estimated power output per day in March.

Date	1	2	3	4	5	6	7	8	9	10	11
Average wind speed (m/s)	2.2	2.6	3.2	1.8	3.0	2.9	2.8	3.3	3.4	4.2	4.2
Main wind direction	NE	SE	E	NNW	NNW	WNW	WNW	SSW	W	SSW	SW
Estimated power output (kWh)	0.11	0.19	0.35	0.06	0.29	0.26	0.23	0.38	0.42	0.79	0.79
Date	12	13	14	15	16	17	18	19	20	21	22
Average wind speed (m/s)	3.5	4.0	2.5	4.6	5.7	5.5	6.6	3.6	3.0	3.3	3.8
Main wind direction	SW	SW	NW	SW	W	SW	SW	NE	N	N	SSW
Estimated power output (kWh)	0.46	0.68	0.17	1.04	1.97	1.77	3.06	0.50	0.29	0.38	0.58
Date	23	24	25	26	27	28	29	30	31		
Average wind speed (m/s)	3.6	5.1	3.9	3.3	1.9	4.0	3.4	2.1	2.1	-	-
Main wind direction	SSW	SSW	SW	W	NNW	SW	WSW	ESE	SSW	-	-
Estimated power output (kWh)	0.50	1.41	0.63	0.38	0.07	0.68	0.42	0.10	0.10	-	-

Table A4. Estimated power output per day in April.

Date	1	2	3	4	5	6	7	8	9	10	11
Average wind speed (m/s)	1.8	1.4	2.4	3.7	3.5	3.7	2.9	2.7	3.0	4.0	2.4
Main wind direction	SSW	SSW	SSW	SSW	N	SW	SSW	SSW	SSW	NW	NE
Estimated power output (kWh)	0.06	0.03	0.15	0.54	0.46	0.54	0.26	0.21	0.29	0.68	0.15
Date	12	13	14	15	16	17	18	19	20	21	22
Average wind speed (m/s)	2.3	3.0	2.8	3.2	3.5	3.6	3.4	4.4	3.3	2.3	2.2
Main wind direction	NE	NE	SE	SSW	SSW	SW	NE	NE	ESE	SSW	SE
Estimated power output (kWh)	0.13	0.29	0.23	0.35	0.46	0.50	0.42	0.91	0.38	0.13	0.11
Date	23	24	25	26	27	28	29	30			
Average wind speed (m/s)	2.7	1.6	1.4	2.2	2.1	4.2	3.1	2.2	-	-	-
Main wind direction	N	SSW	SSW	SSW	SW	E	SSW	ESE	-	-	-
Estimated power output (kWh)	0.21	0.04	0.03	0.11	0.10	0.79	0.32	0.11	-	-	-

Table A5. Estimated power output per day in May.

Date	1	2	3	4	5	6	7	8	9	10	11
Average wind speed (m/s)	3.6	4.1	4.2	3.9	3.5	4.0	5.3	5.3	2.9	3.1	2.8
Main wind direction	SSW	SW	WNW	SW	WSW	SW	WSW	SW	ESE	ESE	SSW
Estimated power output (kWh)	0.50	0.73	0.79	0.63	0.46	0.68	1.58	1.58	0.26	0.32	0.23
Date	12	13	14	15	16	17	18	19	20	21	22
Average wind speed (m/s)	5.2	4.1	2.5	3.1	3.5	2.5	1.9	1.7	1.9	2.5	2.9
Main wind direction	WSW	SSW	SSW	N	SSW	SSW	SE	SSW	NE	SSW	SE
Estimated power output (kWh)	1.50	0.73	0.17	0.32	0.46	0.17	0.07	0.05	0.07	0.17	0.26
Date	23	24	25	26	27	28	29	30	31		
Average wind speed (m/s)	2.4	4.3	5.4	4.4	5.8	4.7	3.6	3.6	3.0	-	-
Main wind direction	ESE	SSW	SSW	SW	W	SW	SSW	SSW	SSW	-	-
Estimated power output (kWh)	0.15	0.85	1.68	0.91	2.08	1.11	0.50	0.50	0.29	-	-

Table A6. Estimated power output per day in June.

Date	1	2	3	4	5	6	7	8	9	10	11
Average wind speed (m/s)	2.8	2.4	2.8	3.5	3.2	1.9	2.5	2.1	2.7	3.0	3.1
Main wind direction	SSW	WSW	NE	NE	NE	SE	SE	SE	E	NE	NE
Estimated power output (kWh)	0.23	0.15	0.23	0.46	0.35	0.07	0.17	0.10	0.21	0.29	0.32
Date	12	13	14	15	16	17	18	19	20	21	22
Average wind speed (m/s)	2.2	3.3	3.4	3.5	3.8	2.1	3.0	3.0	2.9	3.5	2.7
Main wind direction	SE	SSW	SW	SW	SSW	SSW	NNE	SSW	ESE	NE	NNE
Estimated power output (kWh)	0.11	0.38	0.42	0.46	0.58	0.10	0.29	0.29	0.26	0.46	0.21
Date	23	24	25	26	27	28	29	30			
Average wind speed (m/s)	2.3	2.6	2.5	2.8	2.4	3.5	3.1	2.5	-	-	-
Main wind direction	SSW	SSW	SSW	SSW	ESE	SW	SSW	SSW	-	-	-
Estimated power output (kWh)	0.13	0.19	0.17	0.23	0.15	0.46	0.32	0.17	-	-	-

Table A7. Estimated power output per day in July.

Date	1	2	3	4	5	6	7	8	9	10	11
Average wind speed (m/s)	2.5	2.0	2.6	1.9	1.9	2.4	1.9	1.3	3.4	2.6	3.2
Main wind direction	SSW	SE	NE	SE	E	ESE	NE	WNW	E	NNE	WSW
Estimated power output (kWh)	0.17	0.09	0.19	0.07	0.07	0.15	0.07	0.02	0.42	0.19	0.35
Date	12	13	14	15	16	17	18	19	20	21	22
Average wind speed (m/s)	3.3	2.7	3.7	3.1	3.1	3.4	3.6	3.3	2.1	3.1	5.5
Main wind direction	SSW	NNW	SSW	SSW	SSW	SW	N	W	NW	SSW	SW
Estimated power output (kWh)	0.38	0.21	0.54	0.32	0.32	0.42	0.50	0.38	0.10	0.32	1.77
Date	23	24	25	26	27	28	29	30	31		
Average wind speed (m/s)	5.3	5.0	6.0	7.6	2.6	2.3	2.4	1.7	2.3	-	-
Main wind direction	SSW	SW	SW	SW	ESE	ESE	SSW	ESE	ESE	-	-
Estimated power output (kWh)	1.58	1.33	2.30	4.67	0.19	0.13	0.15	0.05	0.13	-	-

Table A8. Estimated power output per day in August.

Date	1	2	3	4	5	6	7	8	9	10	11
Average wind speed (m/s)	3.4	4.9	5.9	7.2	4.0	3.6	2.6	4.1	5.0	2.9	2.7
Main wind direction	ENE	ESE	SSW	SW	SW	SSW	S	NE	NNE	NNE	SW
Estimated power output (kWh)	0.42	1.25	2.19	3.97	0.68	0.50	0.19	0.73	1.33	0.26	0.21
Date	12	13	14	15	16	17	18	19	20	21	22
Average wind speed (m/s)	2.9	1.5	3.3	2.2	2.3	2.9	4.2	4.2	3.1	5.9	3.3
Main wind direction	S	SSW	NE	NW	ESE	ENE	SW	SW	SSW	SW	WSW
Estimated power output (kWh)	0.26	0.04	0.38	0.11	0.13	0.26	0.79	0.79	0.32	2.19	0.38
Date	23	24	25	26	27	28	29	30	31		
Average wind speed (m/s)	3.4	2.4	3.2	2.7	3.0	2.7	2.9	2.9	2.7	-	-
Main wind direction	SSW	SSW	SSE	SSW	NE	NNE	NE	NE	NE	-	-
Estimated power output (kWh)	0.42	0.15	0.35	0.21	0.29	0.21	0.26	0.26	0.21	-	-

Table A9. Estimated power output per day in September.

Date	1	2	3	4	5	6	7	8	9	10	11
Average wind speed (m/s)	3.0	3.0	4.8	3.9	2.7	2.1	1.9	2.4	2.4	2.8	3.2
Main wind direction	E	NE	SW	W	SSW	SSW	ESE	ESE	SSW	ESE	E
Estimated power output (kWh)	0.29	0.29	1.18	0.63	0.21	0.10	0.07	0.15	0.15	0.23	0.35
Date	12	13	14	15	16	17	18	19	20	21	22
Average wind speed (m/s)	2.6	3.4	2.9	1.9	2.4	1.8	2.9	2.5	2.8	2.7	3.0
Main wind direction	ENE	E	E	NNW	NW	ESE	NE	E	E	ESE	E
Estimated power output (kWh)	0.19	0.42	0.26	0.07	0.15	0.06	0.26	0.17	0.23	0.21	0.29
Date	23	24	25	26	27	28	29	30			
Average wind speed (m/s)	3.0	3.6	2.3	3.0	1.9	2.0	2.4	3.2	-	-	-
Main wind direction	ENE	SSW	NE	ENE	SSW	ESE	SE	NE	-	-	-
Estimated power output (kWh)	0.29	0.50	0.13	0.29	0.07	0.09	0.15	0.35	-	-	-

Table A10. Estimated power output per day in October.

Date	1	2	3	4	5	6	7	8	9	10	11
Average wind speed (m/s)	2.9	2.9	2.7	4.5	4.7	3.2	2.4	1.9	2.9	3.0	5.0
Main wind direction	NE	SSW	N	NE	NE	N	SE	E	SE	NE	NE
Estimated power output (kWh)	0.26	0.26	0.21	0.97	1.11	0.35	0.15	0.07	0.26	0.29	1.33
Date	12	13	14	15	16	17	18	19	20	21	22
Average wind speed (m/s)	4.1	5.3	3.0	2.3	3.4	2.3	1.6	1.1	3.9	3.2	4.2
Main wind direction	NE	NE	NE	SSW	WNW	NNW	NW	ESE	WSW	NE	NE
Estimated power output (kWh)	0.73	1.58	0.29	0.13	0.42	0.13	0.04	0.01	0.63	0.35	0.79
Date	23	24	25	26	27	28	29	30	31		
Average wind speed (m/s)	2.3	3.0	2.8	3.1	2.7	1.3	1.1	1.6	2.2	-	-
Main wind direction	NNE	NNW	SSW	WSW	N	SSW	SSE	ESE	ENE	-	-
Estimated power output (kWh)	0.13	0.29	0.23	0.32	0.21	0.02	0.01	0.04	0.11	-	-

Table A11. Estimated power output per day in November.

Date	1	2	3	4	5	6	7	8	9	10	11
Average wind speed (m/s)	2.0	4.1	2.5	2.0	1.7	1.7	2.9	2.0	2.4	1.7	1.8
Main wind direction	NNW	W	WNW	NNW	SSW	NNW	N	NNW	NNW	ESE	W
Estimated power output (kWh)	0.09	0.73	0.17	0.09	0.05	0.05	0.26	0.09	0.15	0.05	0.06
Date	12	13	14	15	16	17	18	19	20	21	22
Average wind speed (m/s)	5.6	4.0	2.5	2.3	2.4	2.7	3.8	2.2	2.2	2.2	1.4
Main wind direction	WNW	WNW	W	NNW	NNW	WNW	NNW	NNW	NNW	SSW	NNW
Estimated power output (kWh)	1.87	0.68	0.17	0.13	0.15	0.21	0.58	0.11	0.11	0.11	0.03
Date	23	24	25	26	27	28	29	30			
Average wind speed (m/s)	1.8	2.6	3.8	2.5	1.1	2.4	2.7	2.2	-	-	-
Main wind direction	NE	NE	NE	NNE	SSW	W	NNW	NNW	-	-	-
Estimated power output (kWh)	0.06	0.19	0.58	0.17	0.01	0.15	0.21	0.11	-	-	-

Table A12. Estimated power output per day in December.

Date	1	2	3	4	5	6	7	8	9	10	11
Average wind speed (m/s)	6.1	4.4	5.7	3.3	3.7	3.7	2.4	2.8	3.0	1.9	3.7
Main wind direction	WNW	WNW	WSW	W	WNW	N	NNW	NNW	NNW	NNW	NNW
Estimated power output (kWh)	2.42	0.91	1.97	0.38	0.54	0.54	0.15	0.23	0.29	0.07	0.54
Date	12	13	14	15	16	17	18	19	20	21	22
Average wind speed (m/s)	3.7	3.1	2.4	1.9	5.2	4.3	2.9	1.8	2.3	2.9	4.0
Main wind direction	NNW	WNW	WNW	SW	WNW	N	W	SSW	WNW	W	W
Estimated power output (kWh)	0.54	0.32	0.15	0.07	1.50	0.85	0.26	0.06	0.13	0.26	0.68
Date	23	24	25	26	27	28	29	30	31		
Average wind speed (m/s)	3.4	3.2	2.3	3.1	1.2	3.7	2.6	3.9	4.1	-	-
Main wind direction	W	WSW	WNW	NNW	NNW	NW	N	W	WNW	-	-
Estimated power output (kWh)	0.42	0.35	0.13	0.32	0.02	0.54	0.19	0.63	0.73	-	-

References

1. *Global Wind Report Annual Market Update 2012*; Global Wind Energy Council (GWEC): Brussels, Belgium, 2012.
2. Delucchi, M.A.; Jacobson, M.Z. Providing all global energy with wind, water, and solar power, Part II: Reliability, system and transmission costs, and policies. *Energy Policy* **2011**, *39*, 1170–1190.
3. Nakamura, Y.; Oke, T.R. Wind, temperature and stability conditions in an east-west oriented urban canyon. *Atmos. Environ.* **1988**, *22*, 2691–2700.
4. Lu, L.; Ip, K.Y. Investigation on the feasibility and enhancement methods of wind power utilization in high-rise buildings of Hong Kong. *Renew. Sustain. Energy Rev.* **2009**, *13*, 450–461.
5. Tsanga, C.W.; Kwoka, K.C.S.; Hitchcock, P.A. Wind tunnel study of pedestrian level wind environment around tall buildings: Effects of building dimensions, separation and podium. *Build. Environ.* **2012**, *49*, 167–181.
6. Hartman, J. Researchers study potential of wind-powered buildings. *Civil Eng.* **2001**, *71*, 13.
7. *Urban Aerodynamics: Wind Engineering for Urban Planners and Designers*; American Society of Civil Engineers (ASCE): Reston, VA, USA, 2011.
8. Grant, A.; Johnstone, C.; Kelly, N. Urban wind energy conversion: The potential of ducted turbines. *Renew. Energy* **2008**, *33*, 1157–1163.
9. Manwell, J.F.; McGowan, J.G.; Rogers, A.L. *Wind Energy Explained: Theory, Design and Application*, 2nd ed.; Wiley: Chichester, UK, 2009.
10. Tzempelikos, A.; Athienitis, A.K. The impact of shading design and control on building cooling and lighting demand. *Sol. Energy* **2007**, *81*, 369–382.
11. Lee, J.W.; Jung, H.J.; Park, J.Y.; Lee, J.B.; Yoon, Y. Optimization of building window system in Asian regions by analyzing solar heat gain and daylighting elements. *Renew. Energy* **2013**, *50*, 522–531.
12. Ushiyama, I.; Nagai, H. Optimum design configuration and performance of Savonius rotors. *Wind Eng.* **1988**, *12*, 59–75.
13. Akwa, J.V.; Vielmo, H.A.; Petry, A.P. A review on the performance of Savonius wind turbines. *Renew. Sustain. Energy Rev.* **2012**, *16*, 3054–3064.
14. Blocken, B.; Carmeliet, J. Pedestrian Wind Environment around Buildings: Literature Review and Practical Examples. *J. Ther. Envel. Build. Sci.* **2004**, *28*, 107–159.
15. Shikha, S.; Bhatti, T.S.; Kothari, D.P. Vertical axis wind rotor with concentration by convergent nozzles. *Wind Eng.* **2003**, *27*, 555–559.
16. Hua, S.Y.; Cheng, J.H. Innovatory designs for ducted wind turbines. *Renew. Energy* **2008**, *33*, 1491–1498.
17. Chong, W.T.; Pan, K.C.; Poh, S.C.; Fazlizan, A.; Oon, C.S.; Badarudin, A.; Nik-Ghazali, N. Performance investigation of a power augmented vertical axis wind turbine for urban high-rise application. *Renew. Energy* **2013**, *51*, 388–397.
18. Irabu, K.; Roy, J.N. Characteristics of wind power on Savonius rotor using a guide-box tunnel. *Exp. Ther. Fluid Sci.* **2007**, *32*, 580–586.
19. Kim, D.K.; Kim, M.K.; Cha, D.K.; Yoon, S.H. Design of drag-type vertical axis miniature wind turbine using arc shaped blade. *J. Korean Fluid Mach. Assoc.* **2006**, *9*, 7–12.

20. Park, J.Y.; Lee, M.J.; Lee, S.J.; Lee, S. An experimental study on the aerodynamic performance of high-efficient, small-scale, vertical-axis wind turbine. *Trans. Korean Soc. Mech. Eng. B* **2009**, *33*, 580–588.
21. Dobrev, I.; Massouh, F. CFD and PIV investigation of unsteady flow through Savonius wind turbine. *Energy Procedia* **2011**, *6*, 711–720.
22. Choi, I.Y.; Cho, S.H.; Kim, J.T. Energy consumption characteristics of high-rise apartment buildings according to building shape and mixed-use development. *Energy Build.* **2012**, *46*, 123–131.
23. Korea Meteorological Administration (KMA). Available online: http://www.kma.go.kr/weather/observation/past_tendays.jsp (accessed on 23 September 2015).
24. *Wind Resource Map Research Development Report*; Korea Meteorological Administration (KMA): Seoul, Korea, 2007.